Electronic Supporting Information (ESI)

Vertically aligned ZnO@CuS@PEDOT core@shell nanorod arrays decorated with MnO_2 nanoparticles for high-performance and semi-transparent supercapacitor electrode

Jorge Rodríguez-Moreno,[a] Elena Navarrete-Astorga,[a] Enrique A. Dalchiele,[b] Ricardo Schrebler,[c] José R. Ramos-Barrado[a] and Francisco Martín[a]

a Universidad de Málaga. Andalucía Tech. Departamentos de Física Aplicada & Ingeniería Química. Laboratorio de Materiales y Superficies (Unidad Asociada al CSIC), E29071 Málaga, Spain.

b Instituto de Física, Facultad de Ingeniería, Herrera y Reissig 565, C.C. 30, 11000 Montevideo, Uruguay.

c Instituto de Química, Facultad de Ciencias, Pontificia Universidad Católica de Valparaíso, Casilla 4059, Valparaíso, Chile

1. EXPERIMENTAL DETAILS

Synthesis. 3.5 cm x 1 cm glass sheet substrates coated with a tin-doped indium oxide (ITO) thin film were previously sequentially ultrasonically cleaned in acetone, iso-propanol and finally in distilled water, 5 minutes in each solvent. ZnO nanorods has been grown electrochemically in a conventional three-electrode electrochemical cell following the procedure previously reported.[S1] Copper sulphide was prepared by spray pyrolysis using two aqueous solutions of 0.01M Thiourea and 0.01M copper acetate monohydrate (Sigma-Aldrich). Both solutions were simultaneously and directly sprayed on the sample heated at 250 ºC using two syringe pumps at a rate of 50 ml/h and a auxiliary stream of pressured air of 30l/min and 2 bar. PEDOT thin films have been

grown by electropolymerization of (3,4-ethylene dioxythiophene) (EDOT) monomer by a cycling potential procedure in a conventional three-electrode electrochemical cell. The electrolytic bath was composed of: 3 mM EDOT monomer (Sigma-Aldrich) and 0.2 M lithium perchlorate salt ($LiClO_4$) (Sigma-Aldrich) in a 3:7 acetonitrile:water solution volume ratio. The electrode potential was cycled between -0.8 to 1.2 V vs. a saturated mercury-mercurous sulfate reference electrode (SME) at 75 mVs^{-1} and for 10 cycles. In order to coat the ZnO NR@CuS@PEDOT nanorods with MnO_2 nanoparticles, these samples have been soaked in a 10mM $KMnO_4$ (Sigma-Aldrich) aqueous solution for 10 minutes.

Morphological characterization. Morphological characterization of the ZnO nanorod arrays and the different hybrid nanostructures have been carried out by field emission scanning electron microscopy images (FESEM-FIB. FEI-Helios 650), high resolution transmission electron microscopy (HRTEM Philips CM-200 microscope). Specimens for TEM were prepared by removing the nanostructured grown material by grating with a scalpel, collected and ultrasonically dispersed in 1 ml of ethanol. A small drop of the suspended solution was placed onto a porous carbon film supported on a nickel grid and left dry in air. HRTEM images have been captured with a high speed digital camera TVIPS FastScan F-114 model at 200KV. The chemical composition of the samples was analyzed through a linear energy dispersive X-ray (EDX) spectrometer attached to the HRTEM (Genesis-4000) and SEM-FIB equipment, respectively. Raman spectra were recorded with a combined dispersive Raman spectrometer (SENTERRA) and a confocal microscope (Olympus BX series) device equipped at 532 nm Nd:YAG laser. X-ray Photo-electron Spectroscopy (XPS ESCA 5701 Physical Electronics (PHI)) with a monochromated Mg Kα source at 300W was used to study the state of oxidation of the elements. C 1s at 284.8 eV was established as referenced for charge correction. The

infrared spectra were recorded with a FTIR spectrometer (VERTEX 70) equipped with a Golden Gate Single Reflection Diamond ATR System from Specac. The UV-vis-NIR spectra were recorded using Cary 5000 from Varian spectrometer, only the direct transmittance was measured.

Electrochemical testing. Cyclic Voltammetry (CV), Galvanostatic Charge-Discharge (GCD) and Electrochemical Impedance Spectroscopy (EIS) have been performed in a potentiostic electrochemical workstation (PGSTAT 30 AUTOLAB) at room temperature. A three-electrode cell configuration has been used to evaluate the behavior of the supercapacitor electrode in 1M $LiClO_4$ aqueous solution in a potential range from -55 mV to 50 mV vs. SME. EIS measurements were carried out at 0 V vs. SME by applying a sinusoidal signal of 10 mV amplitude at frequencies ranging from 100 mHz to 10 KHz. The specific areal capacitances were calculated from CV and GCD curves respectively according to the following two equations: (1) $C_s = \int I\,dV/(kVS)$, where the numerator is the integrated area of CV curve in one cycle, the integrate is applied to a half cycle and k, V and S are the scan rate, voltage window and geometrical electrode surface, respectively. (2) $C = {i\Delta t}/{\Delta V}$, where i, Δt and ΔV are the applied geometrical areal discharge current density, charge period of time and voltage windows, respectively. Dielectric relaxation time is determined according to the equation $\tau = 1/2\pi f$, where f is the peak frequency, where the maximum value is reached for the imaginary complex capacitance C''(ω).

By Spray pyrolysis is possible to obtain copper sulphide phases (Cu_xS) with variable stoichiometry by modulation of the substrate temperature. In fact, for substrate temperatures lower than 260 ºC, copper sulfide phases with x values ranging from x=1 to 1.75 are obtained, whereas at higher substrate temperatures copper-rich phases with x

values from x=1.8 to 2 are obtained.[S2-S6] Fig. S1 shows ex situ Raman spectra (in the wavelength region from 300 to 800 cm^{-1}) of a bare ZnO NRs array (spectrum a), and a ZnO NRs array coated by a copper sulfide nanocrystalline layer grown by spray pyrolysis (spectrum b). The peak at 570 cm^{-1} (Fig. S1 spectrum a) is characteristic of the wurtzite structure of the ZnO nanorods.[S7] The sharp peak at 474 cm^{-1} (Fig. S1 spectrum b), which has been assigned to S-S stretching mode indicates that the copper sulphide is present as covellite CuS phase.[S8]

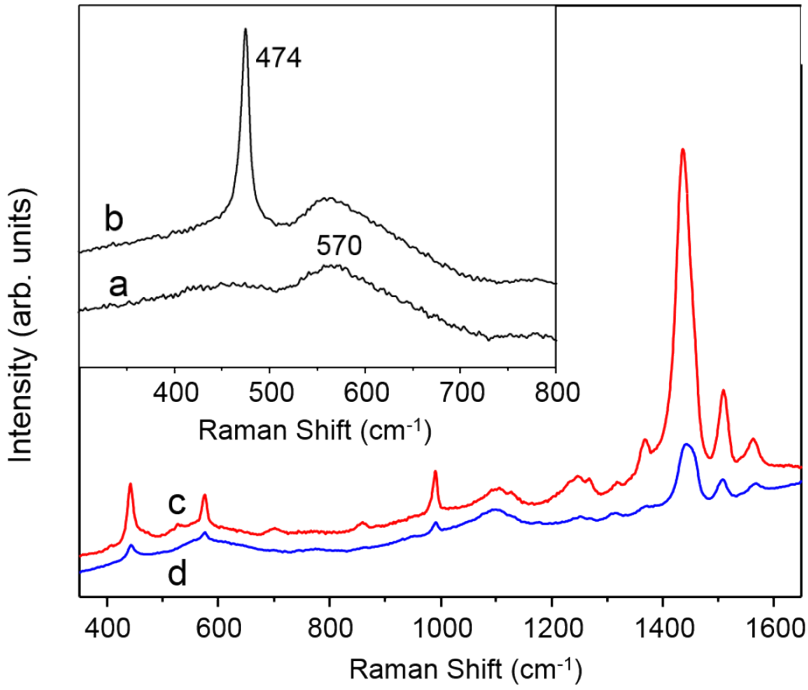

Fig. S1 Ex-situ Raman spectra of different samples recorded at an excitation wavelength of 532 nm: (a) ZnO NRs arrays (b) ZnO NRs@CuS (c) ZnONRs@CuS@PEDOT, (d) ZnO_{NR}@CuS@PEDOT@MnO_2

Raman spectra corresponding to ZnO NRs@CuS@PEDOT and ZnO NRs@PEDOT@MnO_2 samples are displayed in Fig. S1 spectrum *c* and *d*, respectively. According to literature reported data these peaks have been assigned as follow around 440 cm^{-1} to be due to SO_2 bending and at 573 cm^{-1} to C-O-C oxyethylene ring

deformation, at 860 and 990 cm^{-1} to O-C-C and oxyethylene ring deformation respectively;[S8-S10] and peak at 1247, 1370, 1430 and 1507 cm^{-1} correspond to C-C inter-ring stretching, C-C stretching, C=C(-O) stretching, and C=C asymmetric stretching respectively. The similarity of the spectrum of Raman spectrum shown in figure 1 spectrum c with the spectra in the earlier reported studies shows that there is no significant difference between the structures of the PEDOT film obtained in this work with that obtained by other authors.[S9-S11] In Fig. S1, spectrum d, no peaks due to Mn-O stretching vibration have been observed in the region from 500 to 700 cm^{-1},[S12] in part due to the interference of the PEDOT peaks.

The decreasing in the Raman signal in the wavelengths from 1200 to 1600 cm^{-1} would confirm the oxidation process of the polymer through the redox reaction of $KMnO_4$ (oxidation reaction of $KMnO_4$ and its corresponding reduction to MnO_2).[S13] The formation of these MnO_2 nanoparticles has been described elsewhere,[S14] by the reaction illustrated in Fig. S2 and it would have as consequence the oxidation of the thiophene sulfur atom into O=S=O group.

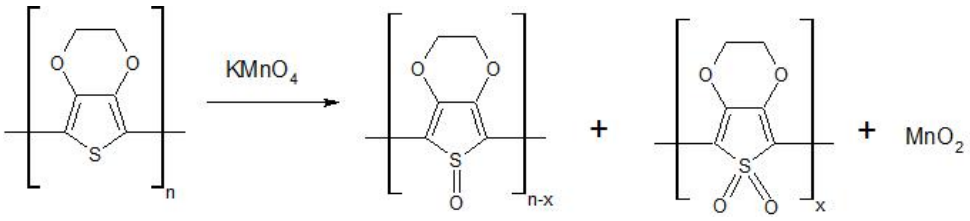

Fig. S2 Reaction occurred between KMnO4 and PEDOT.[S14]

Fig. S3 exhibits the ATR-FTIR ex-situ spectra of a PEDOT layer: as electrodeposited (spectrum a), after being cycled by CV between ±0.4V (spectrum b), and post $KMnO_4$ soaking treatment (spectrum c). In Fig. S3 it can be seen that the spectrum for the PEDOT layer as has been grown by electropolymerization (spectrum a) is in agreement with other published works. [S15-S17]

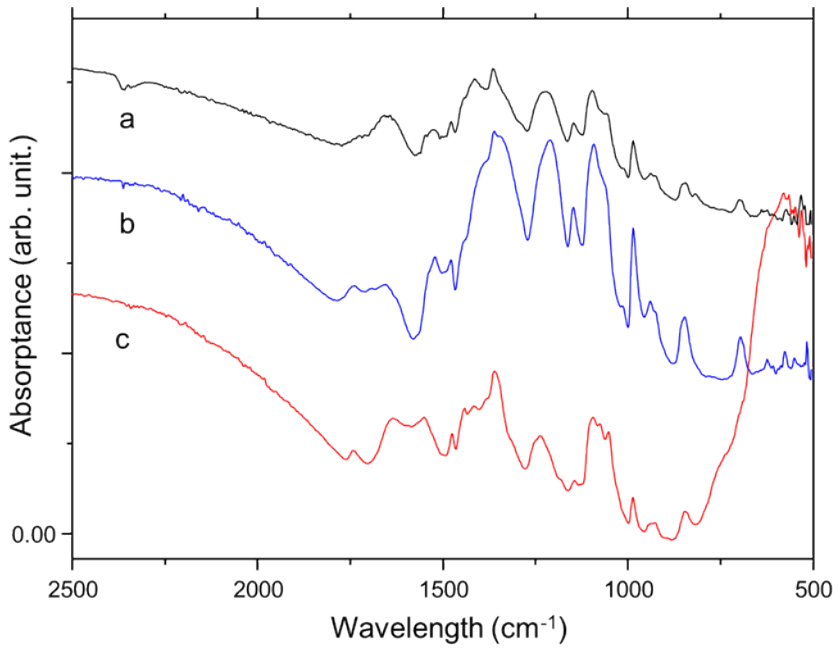

Fig. S3 Ex-situ ATR-FTIR spectra of (a) PEDOT layer as has been grown by electropolymerization. (b) PEDOT layer after being cycled by voltammetry between ±0.4V and (c) PEDOT layer after being soaked in $KMnO_4$ and voltammetric cycled between ±0.4V.

The major characteristic absorption bands for PEDOT are in the range of 1600 – 600 cm^{-1}. The absorption peaks from 1540 to 1300 cm^{-1} are attributed to the stretching modes C=C and C-C of the thiophene ring, whereas the C-O-C bonds stretching in the ethylene dioxy group are linked to the band going from 1300 to 1050 cm^{-1} . Additionally, the stretching bands of C-O-C bond are located at 1085, 1145 and 1210 cm^{-1}. The absorptions due to C-S bond stretching in the thiophene ring are observed as three peaks at 985, 850 and 690 cm^{-1}. The peaks at 959, 872 and 667 cm^{-1} are assigned to C-S bond stretching in the thiophene ring.[S18]

Increasing intensity of peaks at 1357, 1200, 1100 and 980 cm^{-1} for CV cycled PEDOT (Fig. S3 spectrum b) is associated to electron withdrawing in the oxidation process from

the polymer counter ion balancing.[S16] When charge carriers enter the polymer and polarize the polymer backbone the vibrations become IR active due to breaking of the bond symmetry, and are enhanced because the charge distribution causes changes in dipole moments during vibration.[S10] The peak at 1738 cm^{-1} has been related with a doped state of PEDOT.[S18-S19]

The main difference that can be observed for the spectrum after $KMnO_4$ impregnation and potential cyclation is the intense peak at 550 cm^{-1} (Fig. S3 spectrum c), which has been assigned to Mn–O lattice vibrations, which is a proof of the presence of the MnO_2.[S20]

Fig. S4 shows comparatively the spectra of PEDOT as electropolymerized (spectrum a) and after being soaked in a $KMnO_4$ solution and potential cycled by CV (±0.4V) (spectrum b). The absorbance peak at 1351 cm^{-1} (curve c from deconvolution of the spectrum b) grows relatively to the nearest peaks can be assigned to the sulfoxide SO_2 stretching mode, which suggests oxidation of the thiophene sulfur into sulfoxide by $KMnO_4$. Others authors have suggested 1044 cm^{-1}.[S21] The new peak around 1553 cm^{-1} (Fig. S3 curve d) could be attributed to O−H stretching vibrations on a Mn atom and/or to hydrated sulfonate groups.[S22-S23]

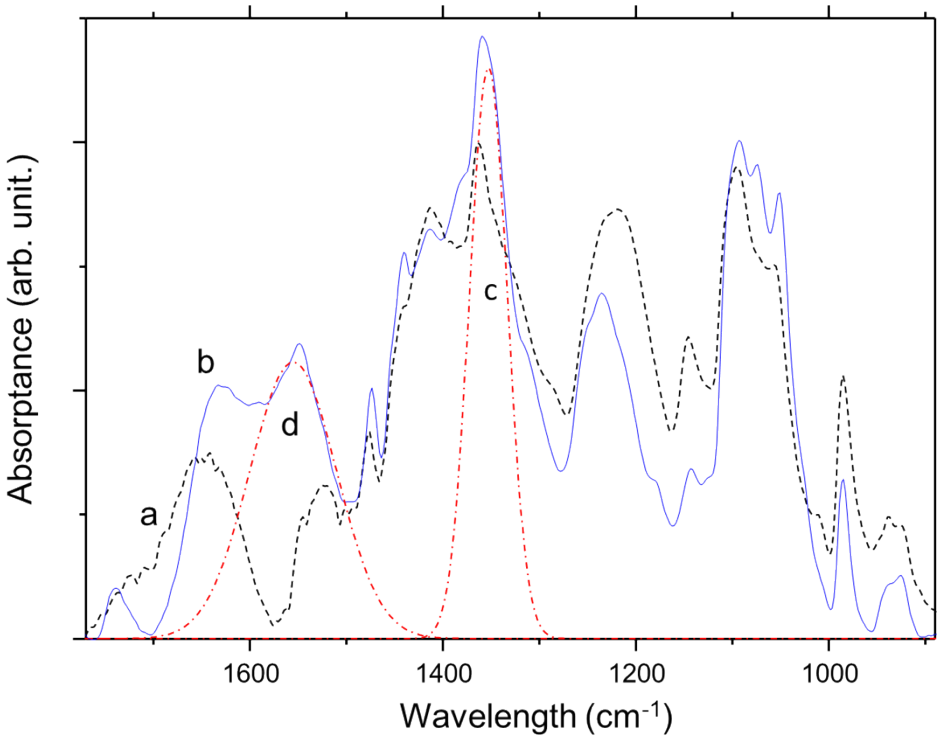

Fig. S4 Ex-situ ATR-FTIR spectra of: (a) a PEDOT layer as electropolymerized and (b) PEDOT layer after being soaked in $KMnO_4$ solution and potential cycled by CV between ±0.4V.

Fig. S5a (spectrum 1) is due to undeconvoluted $S2p_{3/2}$, $S2p_{1/2}$ peaks of CuS (Fig S5c shows the corresponding region of the Cu 2p). As it is known, PEDOT contains one sulfur atom per repeated unit in the thiophene ring. The peak shifts to 163.7 eV for the PEDOT layer (Fig. S5a spectrum 2) corresponds to the spin-split components of the sulfur atoms in PEDOT, but the intensity ratio of the deconvoluted $S2p_{3/2}/S2p_{1/2}$ is not the expected 2/1, which had been reported by others authors.[S24-S26] The binding energies in the range of 163.4–165.6 eV are attributed to S 2p in the C–S bond of PEDOT chains.

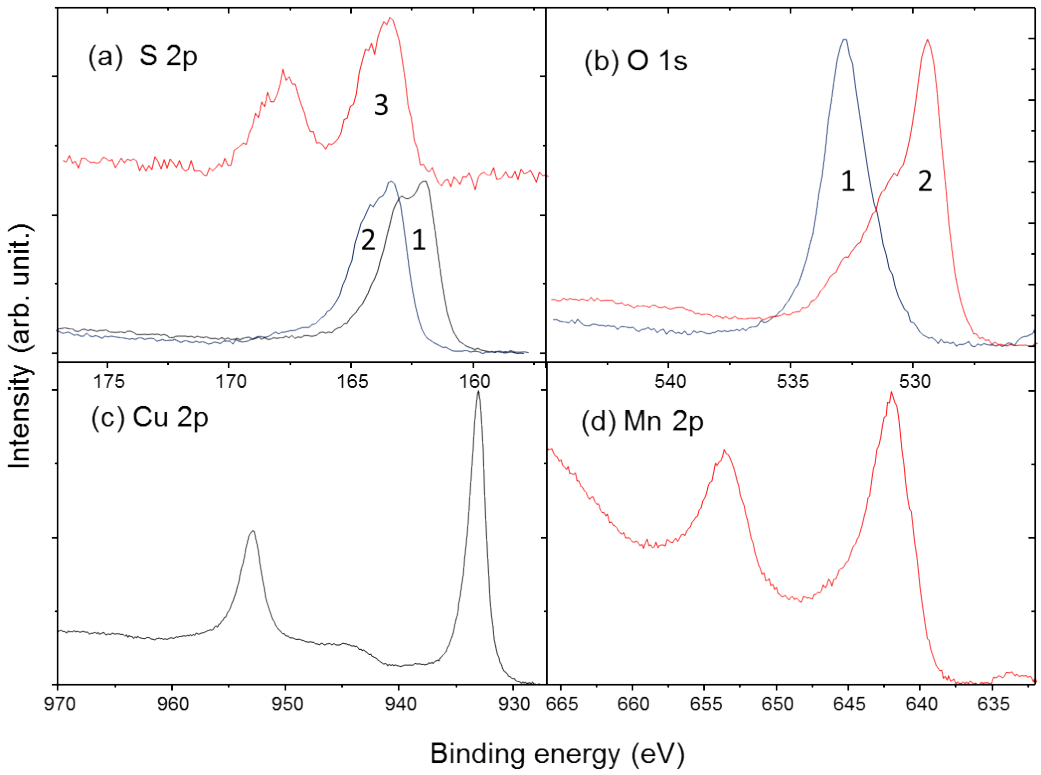

Fig. S5: XPS regions S2p (a): (a-1) ZnO NRs@CuS, (a-2) ZnO NRs@CuS@PEDOT, (a-3) ZnO NRs@CuS@PEDOT@MnO_2. Region O1s (b): (b-1) ZnO NRs@CuS@PEDOT, (b-2) ZnO NRs@CuS@PEDOT@MnO_2. Region Cu2p (c) ZnO

The S 2p region for the PEDOT after being soaked in $KMnO_4$ solution (Fig. S5a spectrum 3) exhibited an increase in intensity in the broad peak near 168 eV. It is an indication of sulphur oxidation of the PEDOT thiophene ring by the $KMnO_4$ according to the Figure S2,[S14] as the peak at 168 eV is attributed to the sulfur in a sulfone group (R-SO_2-R) created upon oxidation.[S27-S29]

Fig. S5d shows the Mn 2p XPS region. The Mn valences of 3^+ and 4^+ have Mn $2p_{3/2}$ and Mn $2p_{1/2}$ binding energy peaks with similar separations, but pure MnO_2 has the $2p_{3/2}$ and $2p_{1/2}$ peaks located at 642 and 653.6 eV (separation of 11.6 eV) which is coincident with the values obtained in the Mn 2p region (Fig. S5d),[S30-S31] and this confirm the presence of MnO_2. Oxygen in MnO_2 is expected to appear at 530 eV (figure 4b-2) .[S30]

Fig. S5b (spectrum 1), shows a peak at 533 eV assigned to the oxygen atoms in the dioxyethylene bridge C-O-C of the PEDOT subunits in the polymer chain.[S25,S32] Deconvolution of spectrum 2 (Fig. S4b) corresponding to the O1s region indicates O–Mn–O (Mn^{4+}) at 530 eV.[S30,S33]

The C 1s region (do not show here) can be deconvoluted in peaks at 284.8 eV assigned to C-C bonding, 285 eV assigned to C-S bonding in the aromatic ring, and a peak at 286 eV attributed to the C-C-O bond.[S34] The C 1s spectrum of the PEDOT exhibits maxima in the range between 284 and 286 eV.

Figures S6 shows the SAED of isolated CuS nanoparticles, the rings and points pattern prove the nano-crystallite nature of the covellite CuS.

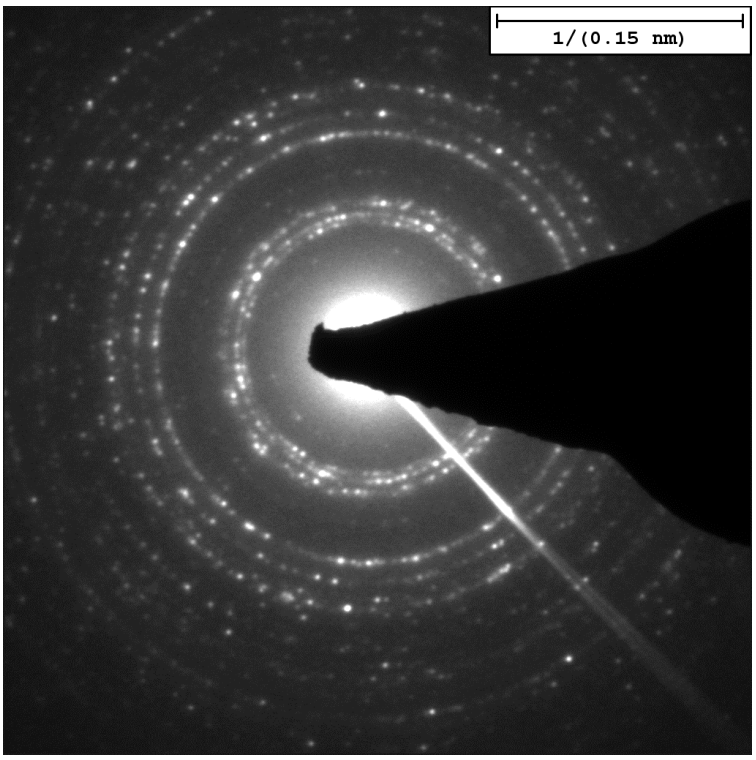

Fig. S6: Selected Area Electron Diffraction (SAED) of a nano-crystallite CuS obtained by spray pyrolysis.

Figure S7, shows a High Resolution TEM image of the outer shell of a NRs@CuS@PEDOT@MnO_2 nanorod. The particles were estimated to be about 5 nm and some crystallographic planes were identified by FFT which appear to be compatible with ramsdellite MnO2 (ICCD *78321), but due to the amount of polymorphs that MnO_2 presents others polymorphs are possible, for example pyrolusite (ICCD*393).

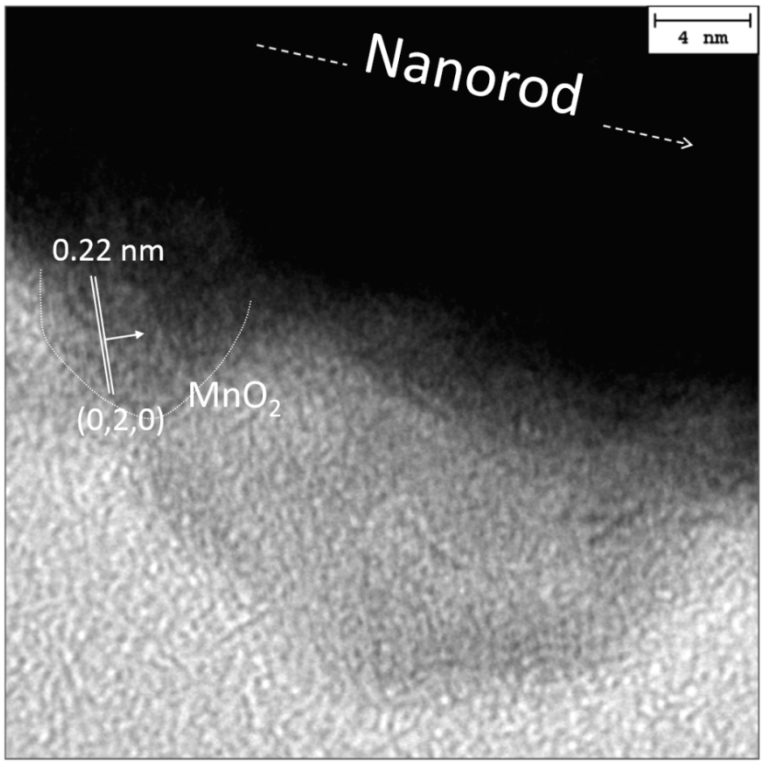

Fig. S7: High Resolution TEM of the outer shell of ZnO NRs@CuS@PEDOT@MnO_2 nanorod

A direct comparison between the performance of planar vs. nanopillar architecture based supercapacitor electrodes has been done. Fig. S8a shows cyclic voltammetric curves for different planar hybrid layered samples (i.e.: PEDOT, CuS@PEDOT, PEDOT@MnO_2 and CuS@PEDOT@MnO_2 grown onto ITO/glass substrates). Clearly, CV curves of supercapacitor electrodes based on planar architectures present deeply distorted shapes compared to those of supercapacitors based on 1D nanostructured structures. As a consequence, lower mass transfer process is associated with the just stated arrangement. On the other hand, Fig. S8b shows comparative cyclic voltammograms for a PEDOT layer and different hybrid 1D nanostructures (i.e.: ZnO NRs@PEDOT, ZnO NRs@CuS@PEDOT and ZnO NRs@CuS@PEDOT@MnO_2) grown onto an ITO/glass substrate, based electrodes. The ZnO NRs@CuS@PEDOT@MnO_2 electrode exhibits a specific areal capacitance of 14.20 mF/cm^2 at 100 mV/s, three times higher than that of a PEDOT planar layer deposited onto an ITO/glass substrate (4.86 mF/cm^2). Improved specific capacitance with the addition of the different materials is in agreement with afore mentioned.

Typical galvanostatic charge-discharge curves at 0.05 mA/cm^2 for a bare and MnO_2 NPs decorated PEDOT planar layer and different hybrid 1D nanostructures (i.e.: ZnO NRs@PEDOT, ZnO NRs@CuS@PEDOT and ZnO NRs@CuS@PEDOT@MnO_2) grown onto an ITO/glass substrate, based electrodes, are given in Fig. S8c. Faradic reaction contributions are observed between 0.45V to 0.5V and -0.4V to -0.55V, attributed to structural evolution of Li_xMnO_2 in successive stages.[S35] Therefore, it is suggested to carry out these experiments between -0.4V to 0.5V, where fast capacitive respond is appreciated. Furthermore, MnO_2 nanoparticles conformation reduce considerably internal resistance (IR drop) associated with metal oxide, preventing intensive volume expansion and facilitating charge/discharge operation.

Electrochemical impedance spectroscopy (EIS) was used to further understand the electrochemical process associated with every coating layer. Fig. S8d displays a Nyquist plot for a PEDOT layer and different hybrid 1D nanostructures (i.e.: ZnO NRs@PEDOT, ZnO NRs@CuS@PEDOT and ZnO NRs@CuS@PEDOT@MnO_2) grown onto an ITO/glass substrate, based electrodes. Increased internal resistance is appreciated as far as ZnO nanowire is introduced, owing to its lower conductivity. Nevertheless, oxidation of PEDOT chain arisen from the inclusion of MnO_2 nanoparticle improves the ultimate internal resistance. Broader semicircle span indicates higher charge transfer resistance (radius of semicircle), corroborating faster polymer pseudocapacitance reactions in regards to MnO_2. Imaginary complex capacitance vs. frequency curve (not shown) confirms an increasing dielectric relaxation time, with the deposition of MnO_2 film, indicating a less power output for this arrangement. On the other hand, knee frequency, which determines the transition between stable double layer and mass transfer process, is of the same order in every sample. Therefore, they begin to exhibit capacitive properties approximately at the same time.

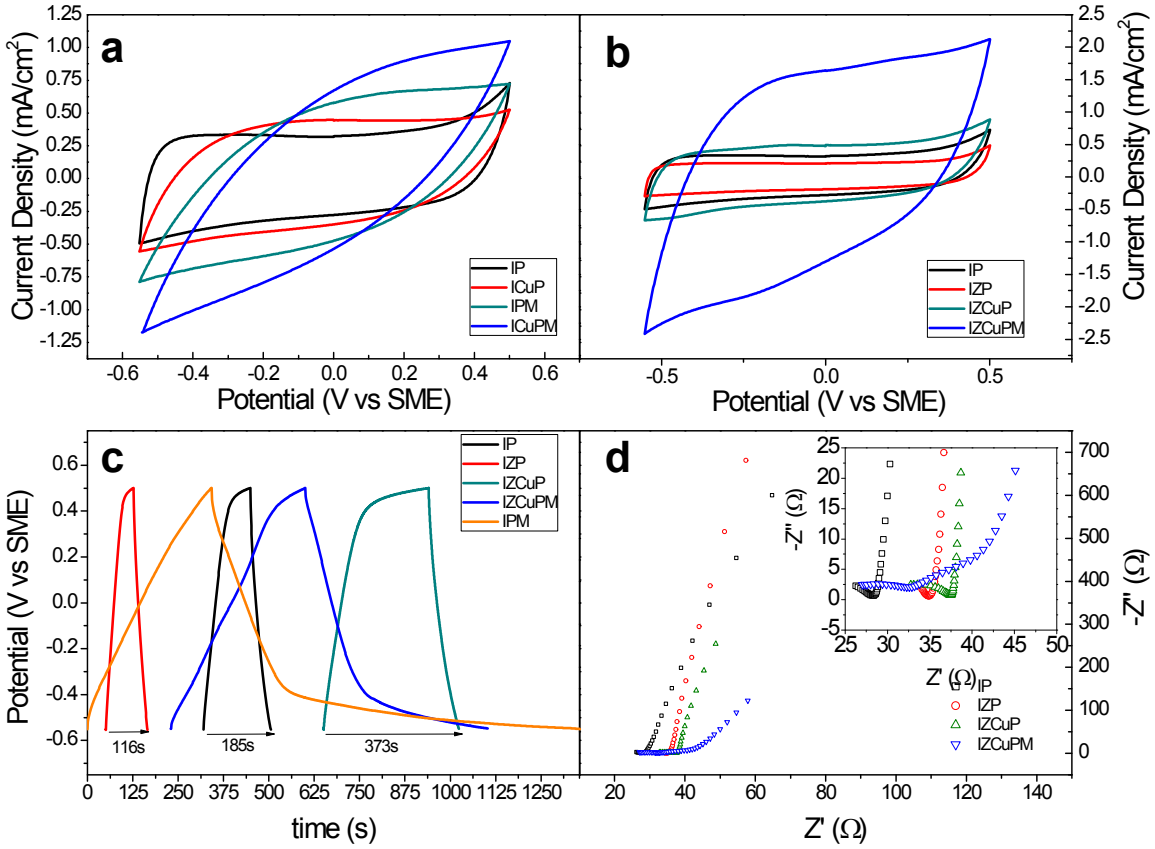

Fig. S8 (a) Cyclic voltammetric curves for different planar hybrid layered samples grown onto ITO/glass substrates: PEDOT (black curve), CuS@PEDOT (red curve), PEDOT@MnO_2 (green curve) and CuS@PEDOT@MnO_2 (blue curve). Scan rate: 100 mV/s. (b) Cyclic voltammograms for a PEDOT layer (black curve) and different hybrid 1D nanostructures: ZnO NRs@PEDOT (red curve), ZnO NRs@CuS@PEDOT (green curve) and ZnO NRs@CuS@PEDOT@MnO_2 (blue curve) grown onto an ITO/glass substrate. Scan rate: 100 mV/s. (c) GCD at 0.05mA/cm^2 and (d) EIS electrochemical performance of a PEDOT layer (black square), and successive deposited nanostructured layers: ZnO NRs@PEDOT (red circle), ZnO NRs@CuS@PEDOT(green triangle) and ZnO NRs@CuS@PEDOT@MnO_2 (blue triangle).

REFERENCES

[S1] J. Rodríguez-Moreno, E. Navarrete-Astorga, R. Romero, F. Martín, R. Schrebler, J. R. Ramos-Barrado and E. A. Dalchiele, *Thin Solid Films*, 2013, **548**, 235

[S2] L. Isac, A. Duta, A. Kriza, S. Manolache and M. Nanu, *Thin Solid Films*, 2007, **515**, 5755.

[S3] C. Nascu , I. Pop, V. Ionescu, I. Bratu, E. Indrea, *Mater. Lett.*, 1997, **32**, 73.

[S4] M.T.S. Nair, L. Guerrero and P.K. Nair, *Semicond. Sci. Technol.*, 1998, **13**, 1164.

[S5] R. Blachnik and A. Müller, *Thermochim. Acta*, 2000, **361**, 31.

[S6] A.U. Ubale, D.M. Choudhari, J.S. Kantale, V.N. Mitkari, M.S. Nikam, W.J. Gawande, and P.P. Patil, *J. Alloys Compd.*, 2011, 509, 9249.

[S7] Z. Zheng-Lin, Z. Gang, Q. Feng-Yuand and W. Xiang, *Chin. Phys. B*, 2012, **21**, 098104.

[S8] M. Ishil, K. Shibata and H. Nozaki, *J. Solid State Chem.*, **1993**,105, 504.

[S9] A. A. Farah, S. A. Rutledge, A. Schaarschmidt, R. Lai, J. P. Freedman and A. S. Helmy, *J. Appl. Phys.*, 2012, **112**, 113709.

[S10] H. Gustafsson, C. Kvarnström and A. Ivaska, *Thin Solid Films*, 2008, **17**, 474.

[S11] B. Zanfrognini, A. Colina, A. Heras, C. Zanardi, R. Seeber and J. López-Palacios, 2011, **96**, 2112.

[S12] K. Rout, M. Mohapatra, S. Anand , *Appl. Surf. Sci.*, **2013**, 270, 205.

[S13] S. Garreau, J. L. Duvail and G. Louarn, *Synth. Met.*, 2002, **125**, 325.

[S14] R. Liu, J. Duay and S. B. Lee, *ACS Nano*, 2010, **4**, 4299.

[S15] Z. Mousavi, T. Alaviuhkola, J. Bobacka, R.-M. Latonen, J. Pursiainen and A. Ivaska, *Electrochim. Acta*, 2008, **53**, 3755.

[S16] C. Kvarnström, H. Neugebauer, S. Blomquist, H. J. Ahonen, J. Kankare and A. Ivaska, *Electrochim. Acta*, 1999, **44**, 2739.

[S17] C. Kvarnström, H. Neugebauer, A. Ivaska and N.S. Sariciftci, *J. Mol. Struct.*, 2000, **521**, 271.

[S18] M. S. Teker, U. Tamer and N. Ö. Pekmez, *Synth. Met.*, **2012**, 162, 924.

[S19] S. V. Selvaganesh, J. Mathiyarasu, K. L. N. Phani and V. Yegnaraman, *Nanoscale Res. Lett.,* 2007, **2**, 546.

[S20] P. Sena, A. De, A. D. Chowdhury, S. K. Bandyopadhyay, N. Agnihotri and M. Mukherjee, *Electrochim. Acta*, 2013, **108**, 265.

[S21] R. Liu and S. B. Lee, *J. Am. Chem. Soc.*, 2008, **130**, 2942.

[S22] Z. Mousavi, T. Alaviuhkola, J. Bobacka, R. M. Latonen, J. Pursiainen and A. Ivaska, *Electrochim. Acta*, 2013, **108**, 265.

[S23] L. Mai, F. Dong, X. Xu, Y. Luo, Q. An, Y. Zhao, J. Pan and J. Yang, *Nano Lett.*, 2013, **13**, 740.

[S24] G. Greczynski, T. Kugler and W. R. Salaneck, *Thin Solid Films*, 1999, **354**, 129.

[S25] G.P. Pandey and A.C. Rastogi, *Electrochim. Acta*, 2013, **87**, 158.

[S26] R. Ruffo, A. Celik-Cochet, U. Posset, C. M. Maria and G. Schottner, *Sol. Energy Mater. Sol. Cells*, 2008, **92**, 140.

[S27] Z. A. King, C. M. Shaw, S. A. Spanninga and D. C. Martin, *Polymer*, 2011, **52**, 1302.

[S28] S. Marciniak, X. Crispin, K. Uvdal, M. Trzcinski, J. Birgerson, L. Groenendaal, F. Louwet and W.R. Salaneck, *Synth. Met.*, 2004, **141**, 67.

[S29] X. Crispin, S. Marciniak, W. Osikowicz, G. Zotti, A. W. Denier Van der Gon, F. Louwet, M. Fahlman, L. Groenendaal, F. de Schryver and W. R. Salaneck, *J. Polym. Sci., Part B: Polym. Phys.*, **2003**, 41 21, 2561.

[S30] J. F Moulder W. F. Stickle, P. E. Sobol and K. D. Bomben, *Handbook of X-ray Photoelectron Spectroscopy* Physical Electronic. Inc. Eden Pradire, Minnesota, 1995.

[S31] M. C. Biesinger, B. P. Payne, A. P. Grosvenor, L. W. M. Lau, A. R. Gerson and R. St.C Smart, *Appl. Surf. Sci.,* 2011**, 257**, 2717.

[S32] S.A. Spanninga, D.C. Martin and Z. Chen, *J. Phys. Chem. C*, 2009, **113**, 5585.

[S33] B. Babakhani and D. G. Ivey, *Electrochim. Acta*, 2010, **55**, 4014.

[S34] A. Lisowska-Oleksiak, A. P. Nowak, M. Wilamowska, M. Sikora, W. Szczerba and C. Kapusta, *Synth. Met.*, 2010, **160**, 1234.

[S35] D. Wang, L-M. Liu, S-J. Zhao, B-H. Li, H. Liu and X-F. Lang, *Phys.Chem. Chem. Phys.*, 2013, **15**, 9075.